

Joint Optimization of Transmission and Propulsion in UAV-Assisted Communication Networks

Omar J. Faqir, Eric C. Kerrigan, Deniz Gündüz, and Yuanbo Nie

Abstract—The communication energy in a wireless network of mobile autonomous agents should be defined to include the propulsion energy as well as the transmission energy used to facilitate information transfer. We therefore develop communication-theoretic and Newtonian dynamic models of the communication and locomotion expenditures of an unmanned aerial vehicle (UAV). These models are used to formulate a novel nonlinear optimal control problem (OCP) for arbitrary networks of autonomous agents. This is the first work to consider mobility as a decision variable in UAV networks with multiple access channels. Where possible, we compare our results with known analytic solutions for particular single-hop network configurations. The OCP is then applied to a multiple-node UAV network for which previous results cannot be readily extended. Numerical results demonstrate increased network capacity and communication energy savings upwards of 70% when compared to more naïve communication policies.

Index Terms—optimal control, predictive control, information theory, wireless networks, unmanned aerial vehicles

I. INTRODUCTION

Unmanned aerial vehicles (UAVs) have diverse potential uses and are currently benefiting from cost reduction and increased on-board compute power. Energy consumption remains a limiting factor, with significant drain from transmission and propulsion energy. In this work we derive a policy for joint control of mobility and transmission to minimize total communication energy in a network. We achieve this by formulating and solving a continuous time nonlinear optimal control problem (OCP). Importantly, we consider communication energy to be the sum of transmission and any propulsion energy used to facilitate communication i.e. when a UAV slows down to maintain access to favourable channels. We develop a general dynamic transmission model based on physical layer communication-theoretic bounds of ergodic and outage

capacities. This is combined with a Newtonian dynamics mobility model and possible network topology.

UAVs can cooperatively complete high-level network objectives, generally including tasks of data gathering/relaying and coordinating movement for the purpose of data gathering/relaying. Data may be collected from the environment (e.g. target tracking, search and pursuit [1], mobile sensor networks [2], [3]) or from other nodes and infrastructure (e.g. using UAVs as supplementary network links [4]). We determine energy-efficient strategies for performing this data gathering and aggregation in a mobile network. Until relatively recently most works regarding node mobility focused on mobile and vehicular ad-hoc networks (MANETs and VANETs respectively), where mobility is either random or largely determined by infrastructure [5]. Since neither MANETs or VANETs are fully autonomous, mobility is typically not a decision variable.

In [6], optimal trajectories are designed for a cellular-enabled UAV to maintain UAV connectivity by formulating the problem as a sequence of cell-tower to UAV associations. A reciprocal problem is addressed in [7], where optimal transport theory is used to derive UAV to cell associations that minimize average network delay for an arbitrary geometry of ground users. For uniformly distributed users, the signal-to-noise (SNR) based association is proven delay-optimal. By the same authors, [8] constructs an analytic framework for rate analysis of terrestrial device-to-device communications overlaid with an interfering UAV network. These works largely neglect UAV mobility dynamics in problem formulations. In formulating our OCP below we will refer further to existing works relating to energy-efficient communication, or relevant transmission and mobility models.

In [9] a single UAV is used as a mobile relay between a stationary source and a sink. For fixed trajectories the throughput maximizing transmission scheme is found analytically, by a directional waterfilling from source to sink. For fixed transmission profile the problem is non-convex and an optimal trajectory is found through a sequence of convex optimizations. By the same authors, [10] develops a method to maximize the throughput per unit of communication energy of a single circular UAV loiter trajectory. As part of an on-line control scheme, [11] uses a linear program (LP) to decide how close a slow rolling-robot should get to its download link before transmitting in order to minimize energy expenditure.

The two user broadcast channel is characterized in [12] for a UAV transmitting independent data to two isolated ground nodes. In particular the hover-fly-hover strategy is shown to be optimal. The trade off between a ground node's communication energy and UAV's propulsion energy is investigated in

©2019 IEEE. Personal use of this material is permitted. Permission from IEEE must be obtained for all other uses, in any current or future media, including reprinting/republishing this material for advertising or promotional purposes, creating new collective works, for resale or redistribution to servers or lists, or reuse of any copyrighted component of this work in other works.

The support of the EPSRC Centre for Doctoral Training in High Performance Embedded and Distributed Systems (HiPEDS, Grant Reference EP/L016796/1) is gratefully acknowledged. D. Gündüz acknowledges funding from the European Research Council through project BEACON (Grant no. 677854).

O. J. Faqir and Deniz Gündüz are with the Department of Electrical & Electronics Engineering, Imperial College London, SW7 2AZ, U.K. ojf12@ic.ac.uk, d.gunduz@ic.ac.uk

Eric C. Kerrigan is with the Department of Electrical & Electronic Engineering and Department of Aeronautics, Imperial College London, London SW7 2AZ, U.K. e.kerrigan@imperial.ac.uk

Yuanbo Nie is with the Department of Aeronautics, Imperial College London, London SW7 2AZ, U.K. yuanbo.nie15@imperial.ac.uk

[13] for the particular case of circular or straight line flights. A pareto boundary is characterised in both cases. Maximizing the minimum throughput between a set of ground users and multiple UAV receivers is investigated in [14]. The problem is initially formulated as a mixed integer nonconvex program. A relaxed nonconvex problem is proposed, and solved through a sequence of block coordinate descent – iterating between trajectory and transmission optimizations – where the former is solved through successive convex optimization. AWGN communication-theoretic bounds are used in [9], [10], [15]. In [9] a single UAV is used as a mobile relay between a stationary source and a sink. For fixed trajectories the throughput-maximizing transmission scheme is obtained analytically by a directional water-filling from source to sink; water-filling is a well-known power allocation scheme for parallel channels [16, Chapter 5] and is further discussed in Section IV-A. On the other hand, for a fixed transmission profile the problem is non-convex and a trajectory is determined iteratively through the solution of a sequence of convex optimizations. The same authors also developed a method to maximize the throughput per unit of communication energy of a single loitering UAV flying at a constant speed [10]. The above works consider restricted cases of the throughput-maximization problem. In the sequel the power minimization problem is addressed.

A predictive channel model accounting for indoor fading dynamics is developed for rolling robotic networks in [17] and employed in [18], [19], but relies on a priori channel measurement. Furthermore, non-convexity is addressed by solving a sequence of appropriately defined convex optimization problems, whereas in this work we generate a control input from formulating a single nonlinear (possibly non-convex) OCP, but leaving it up to the solver as to how best to compute a solution. In our experience with state-of-the-art solvers, such as IPOPT, this can be more efficient than defining a sequence of convex optimization problems a priori.

This work extends [20], [21] by providing supporting analysis of special cases and extending simulation results. In Section II, we formulate the continuous-time OCP for joint optimization of transmission and mobility policies of an arbitrarily-sized network consisting of both static and mobile nodes. The general OCP is non-convex, and will be solved numerically by nonlinear optimization solvers. However, in Section III we present a number of reformulations of the nonlinear constraints and cost that can make the problem easier to solve in practice, as well as a number of special cases under which we can assuredly solve the problem to global optima. In Section IV we analyse simple network configurations in order to gain new insights, and provide a comparison of our results to known solutions. A comparison of energy usage between our proposed scheme and other possible approaches is shown in Section V, before presenting a closed-loop simulation with channel state uncertainty. Even in very simple topologies, savings of upwards of 70% are shown to be possible.

II. SYSTEM MODEL AND PROBLEM FORMULATION

We consider a heterogeneous network of static and mobile nodes that collect/generate data and work cooperatively to

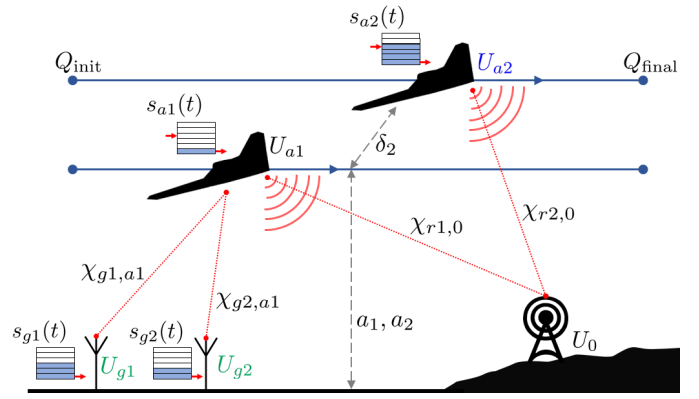


Figure 1: Example system model and geometry for problem formulation. Nodes with *black* fonts will be presented in all our simulations. The node with a *blue* font title is part of the model studied in Section IV-B, while the node with a *green* title is part of the model treated in Section V. The speeds of aerial nodes along these paths are variable and bounded. Solid lines represent the paths of UAV nodes, and red dashed lines correspond to existing communication links across distances χ . Altitudes $a_1, a_2 = 1$ km, and displacement $\delta_2 = 1$ km. For simplicity of exposition, we denote aerial nodes as U_{ai} and ground nodes as U_{gi} , although they are modelled equivalently.

aggregate this data at a specific subset of nodes, such as access points (AP) connected to wired infrastructure. Figure 1 exemplifies the simulation setup, with parameter definitions to follow. Due to complexity issues, most UAV path planning algorithms restrict admissible trajectories to be constant-altitude and either linear or circular [22]. For example, [23] uses nonlinear model predictive control (NMPC) for robust tracking of linear trajectories by fixed-wing UAVs. For simplicity, we therefore consider N (mobile) nodes $U_n, n \in \mathcal{N} \triangleq \{1, \dots, N\}$ travelling along linear non-intersecting trajectories in a Cartesian space. Denote the trajectory of U_n over time interval $\mathcal{T} \triangleq [0, T]$ as $t \mapsto X_n(t) \triangleq (q_n(t), \delta_n, a_n)$, where a_n and δ_n are the constant altitude and lateral displacement, and $q_n(t)$ the time-varying longitudinal displacement of U_n . Over interval \mathcal{T} , each node U_n must travel from position $q_n(0) = Q_{n,\text{init}}$ to $q_n(T) = Q_{n,\text{final}}$. Stationary terrestrial nodes are modelled with $Q_{n,\text{init}} = Q_{n,\text{final}}$, $a_n = 0$. As in [22], we define a trajectory as a time-parameterized path.

At time t , node U_n stores data $s_n(t) \leq M_n$, where M_n denotes the size of the node's on-board memory in bits. All storage buffers are subject to boundary conditions,

$$s_n(0) = D_{n,\text{init}}, \quad s_n(T) \leq D_{n,\text{final}}, \quad \forall n \in \mathcal{N}.$$

Any node U_n may be modelled as an ideal (infinite) sink with $D_{n,\text{final}} = M_n = \infty$. We may for example wish to model the existence of an infrastructure-connected AP in this way.

A. Transmission Model

Wireless communication links may exist from any node U_n to $U_m, \forall n, m \in \mathcal{N}, n \neq m$, over channels with corresponding

gains $h_{mn} \triangleq \nu_{mn}^2$, where ν_{mn} is a realization of the wireless channel gain. We define the link gain from U_n to U_m as

$$\eta_{mn}(\chi_{mn}, h_{mn}) \triangleq \frac{h_{mn} G_{mn}}{\chi_{mn}^\alpha},$$

where $\alpha > 1$ is the path loss exponent, $G_{mn} \triangleq \tilde{G}_{mn} d_0^\alpha$ is a unitless constant of receive and transmit antenna gain \tilde{G}_{mn} at reference distance d_0 , and χ_{mn} is the squared distance between U_n and U_m . We have

$$\chi_{mn}(t) \triangleq \|X_{mn}(t)\|^2 = \|(q_{mn}(t), \delta_{mn}, a_{mn})\|^2,$$

where $q_{mn}(t) \triangleq q_m(t) - q_n(t)$, and δ_{mn}, a_{mn} are similarly defined. At time t , node U_n may transmit to node U_m at a non-negative data rate $r_{mn}(t)$ using associated power $p_{mn}(t)$.

All nodes have a single omnidirectional antenna capable of a maximum transmission power of P_{\max} Watts. We consider the case where an orthogonal frequency bandwidth B_m is assigned for the reception of each node U_m . Each node may receive on its allocated bandwidth, while simultaneously transmitting on other bands. All messages destined for U_m are transmitted over this band, forming a multiple access channel (MAC). We do not allow coding (e.g., network coding) or combining of different data packets at the nodes. Instead, we consider a decode-and-forward-based routing protocol at the relay nodes [24]. The resulting network is a composition of MACs. UAV communication links are typically dominated by line-of-sight (LoS) components, resulting in flat fading channels where all signal components undergo similar amplitude gains [16]. We consider the following channel modelling assumptions:

1) *Additive white Gaussian noise (AWGN)*: The channels between nodes are modelled as scalar AWGN with zero-mean, unit-variance, independent noise components. For a Gaussian MAC the set of achievable rate tuples defines a polymatroid capacity region resulting from the submodularity of mutual information [25]. If N nodes transmit independent information to receiving terminal U_m in the same communication interval, the received signal is a superposition of the N transmitted signals scaled by their respective channel gains $\eta(\chi_{mn}, h_n)$ plus an AWGN term. The set of achievable data rates is evaluated using the Shannon capacity, which is an upper bound on achievable information rates subject to average power constraints. Any rate inside this capacity region may be transmitted with an arbitrarily small probability of error.

The capacity region $\mathcal{C}_{\tilde{\mathcal{N}}}(\cdot)$ of a MAC formed by sources $U_n, n \in \tilde{\mathcal{N}} \subset \mathcal{N}$ and sink $U_m, m \in \mathcal{N} \setminus \tilde{\mathcal{N}}$ denotes the set of achievable rate tuples r , and is defined as

$$\mathcal{C}_{\tilde{\mathcal{N}}}(\chi, p, h) \triangleq \left\{ r \geq 0 \mid f_m(\chi, p, r, h, \mathcal{S}) \leq 0, \forall \mathcal{S} \subseteq \tilde{\mathcal{N}} \right\}, \quad (1)$$

where χ is the tuple of distances χ_{mn} between the $\tilde{\mathcal{N}}$ users and U_m , $p \in \mathcal{P}^N$ is the N -tuple of transmission powers allocated by the N users on the channel reserved for node U_m , with $\mathcal{P} \triangleq [0, P_{\max}]$ being the range of possible transmission powers

for each user. $\mathcal{C}_{\tilde{\mathcal{N}}}(\cdot)$ is bounded from above by $2^{\text{card}(\tilde{\mathcal{N}})} - 1$ nonlinear submodular functions

$$f_m(\chi, p, r, h, \mathcal{S}) \triangleq \sum_{n \in \mathcal{S}} r_n - B_m \log_2 \left(1 + \sum_{n \in \mathcal{S}} \frac{\eta_{mn}(\chi_{mn}, h_{mn}) p_n}{\sigma_m^2} \right), \quad (2)$$

where r_n is the n^{th} component of r , $\sigma_m^2 = 1$ is the receiver noise power and the channel gain $h_{mn} = 1$ for AWGN channels. Convexity of this region implies that throughput maximization does not require time-sharing between nodes, and can be achieved through the decoding process of successive interference cancellation (SIC) [25]. Since the channels are time-invariant, nodes are assumed to have perfect information regarding link status.

2) *Slow fading channel*: In a slow fading channel, the actual channel gains are random but remain constant over a certain communication interval, called the channel coherence time. Considering (1) with random vector h , we see that $\mathcal{C}_{\tilde{\mathcal{N}}} = \emptyset$ with nonzero probability (assuming the transmitter has no channel state information; and hence, cannot perform power allocation). Regardless of the transmission power and distance, it is impossible to guarantee successful transmission at any strictly positive rate with zero probability of error¹ [16]. As such it is no longer reasonable to model rates, power and distance using the capacity formulation in (2).

Often the channel distribution is known or may be estimated, even if the actual channel state h is unknown. In this case we propose a more useful performance measure, the ϵ -outage capacity $\mathcal{C}_{\tilde{\mathcal{N}}}^\epsilon$, defined as the set of achievable rates that guarantee a maximum outage probability of ϵ , namely

$$\mathcal{C}_{\tilde{\mathcal{N}}}^\epsilon \triangleq \mathcal{C}_{\tilde{\mathcal{N}}}(\chi, p, F_h^{-1}(1 - \epsilon)),$$

where F_h is the complementary cumulative distribution of h , $F_h(x) \triangleq \Pr\{h \geq x\}$ [16]. In doing so we are performing chance-constrained optimization. However, because the probability density of h is known, the problem may be written in a deterministic form with no additional complexity [26].

B. Propulsion Model

In [11], [27], [28] the propulsion power required for a rolling-robot is modelled, respectively, as a linear function of speed, polynomial function of speed, and posynomial function of speed and acceleration. This posynomial model is further used in [18], [19] for on-line communication and trajectory co-optimization. Where non-convexity is present, these works propose solving a series of successive convex problems, rather than the original problem. We instead consider a fixed-wing UAV U_n , which is restricted to moving at positive speeds $v_n \in \mathcal{V}_n \triangleq [\underline{V}_n, \bar{V}_n]$, where $0 < \underline{V}_n \leq \bar{V}_n$. $D(\cdot)$ models the resistive forces on U_n , satisfying the following assumption:

Assumption 1. *The resistive forces acting on node U_n may be modeled by the function $v \mapsto D(v)$ such that $v \mapsto vD(v)$*

¹This is under the assumption that h_n cannot be bounded below by a positive value with probability 1, that is, $P\{h_n \leq \epsilon\} > 0, \forall \epsilon > 0$.

is convex on the domain of admissible speeds $v \in \mathcal{V}_n$ and ∞ on $v \notin \mathcal{V}_n$.

The propulsion force $F_n(\cdot)$ generated by the UAV must satisfy the Newtonian dynamic force balance equation

$$F_n(t) - D(v_n(t)) = m_n a_n(t),$$

where m_n is the mass of the UAV U_n , $v_n(t)$ is its speed, and $a_n(t) \triangleq \dot{v}_n(t)$ is its acceleration along the direction of motion at time t . The instantaneous power used for propulsion is the product $F_n(t)v_n(t)$, while the total propulsion energy is the integral of power over time [10]. For a fixed-wing UAV $v_n(t) \gg 0, \forall t \in \mathcal{T}$, whilst for a stationary terrestrial node $v_n(t) = \underline{V}_n = \bar{V}_n = 0, \forall t \in \mathcal{T}$.

The drag force $D(v)$ of a fixed-wing UAV travelling at constant altitude and sub-sonic speed v is modelled [9] as the sum of parasitic and lift-induced drag

$$D(v) = \frac{\rho C_{D0} S v^2}{2} + \frac{2L^2}{(\pi e_0 A_R) \rho S v^2}. \quad (3)$$

In (3), parasitic drag is proportional to the square of the speed, where ρ is air density, C_{D0} is the zero lift drag coefficient, and S is the wing area. Lift-induced drag is inversely proportional to speed squared, where e_0 is the Oswald efficiency factor, A_R the wing aspect ratio, and L the lift force [29]. For level flight, L equals the weight of the aircraft $W = mg$.

Motivated by [10] and in agreement with Assumption 1, we model the resistive forces acting on the UAVs as

$$D(v) \triangleq \begin{cases} C_{D1} v^2 + C_{D2} v^{-2}, & \forall v \in \mathcal{V}, \\ \infty, & \text{otherwise} \end{cases} \quad (4)$$

where we have taken $C_{D1} = 9.26 \times 10^{-4}$ and $C_{D2} = 2250$ for our simulations, as in [10].

Although we specifically consider fixed-wing UAVs due to higher energy efficiency, rotor-craft may have practical advantages due to their ability to hover. In [30] the energy used by a rotary craft moving at constant speed v is decoupled as the sum of vertical and horizontal components. Vertical power depends on the UAV mode of operation (climbing, descending, or descending in windmill state). Assumption 1 is not satisfied in this case, since drag is not a smooth function of speed.

C. Continuous-Time Optimal Control Problem Formulation

Optimization is performed over the tuple of state and control variables which are denoted, for $U_n, n \in \mathcal{N}$, by $Y_n \triangleq (p_n, r_n, s_n, q_n, v_n, a_n, F_n)$, where p_n is the tuple of outgoing transmission powers $p_{mn}(t), \forall m \in \mathcal{N} \setminus \{n\}$, and r_n is the tuple of associated rates r_{mn} . The continuous-time OCP is

$$\min_{Y_n, n \in \mathcal{N}} \sum_{n=1}^N \int_0^T p_n(t) + v_n(t) F_n(t) dt \quad (5a)$$

s.t. $\forall n, m \in \mathcal{N}, t \in \mathcal{T}, \mathcal{S} \subseteq \mathcal{N}$

$$f_m(\chi(t), p(t), r(t), \tilde{h}, \mathcal{S} \setminus \{m\}) \leq 0 \quad (5b)$$

$$\chi_{mn}(t) = \|X_{mn}(t)\|^2 \quad (5c)$$

$$\dot{s}_n(t) = \sum_{m \neq n} (r_{nm}(t) - r_{mn}(t)) \quad (5d)$$

$$s_n(0) = D_{n,\text{init}}, \quad s_n(T) = D_{n,\text{final}} \quad (5e)$$

$$F_n(t) - D(v_n(t)) = m_n a_n(t) \quad (5f)$$

$$\dot{q}_n(t) = \Upsilon_n v_n(t) \quad (5g)$$

$$\dot{v}_n(t) = a(t) \quad (5h)$$

$$q_n(0) = Q_{n,\text{init}}, \quad q_n(T) = Q_{n,\text{final}} \quad (5i)$$

$$v_n(0) = v_{n,\text{init}}, \quad v_n(T) = v_{n,\text{final}} \quad (5j)$$

$$\underline{Y}_n \leq Y_n(t) \leq \bar{Y}_n \quad (5k)$$

The cost function (5a) is the sum of communication energy of all the nodes. Dynamic stage constraints (5b)–(5c) bound the achievable data rates of each MAC to within the polymatroid capacity region of each receiving node. $\tilde{h} = 1$ for AWGN channels and $F^{-1}(1 - \epsilon)$ for slow fading channels. Stage constraint (5f) enforces the force balance condition. System dynamics are included in (5d)–(5h), where (5d) specifically updates data buffers with sent, received and collected data. $\Upsilon_n \in \{-1, 1\}$ depending on if position $q_n(t)$ decreases or increases respectively, because the speed $v_n(t) \geq 0$.

Boundary conditions (5e)–(5j) provide initial and final conditions on the state of the network. With reference to the discussion in Section I, terminal constraints may be interpreted as the higher level objectives: by time $t = T$ all nodes must reach certain positions, and data must have been aggregated to certain nodes. The simple bounds in (5k) are given by

$$\underline{Y}_n \triangleq (0, 0, 0, -\infty, \underline{V}_n, -\infty, \underline{F}),$$

$$\bar{Y}_n \triangleq (P_{\max}, \infty, M, \infty, \bar{V}_n, \infty, \bar{F}),$$

where $0 \leq \underline{V}_n \leq \bar{V}_n$ and $\underline{F} \leq \bar{F}$. The OCP can be discretized and solved using optimal control software, e.g. ICLOCS [31].

Since no explicit routing is performed, the number of capacity region constraints is combinatorial in \mathcal{N} . However, the complexity is not exponential in the absolute size of the network, but in the subset of nodes transmitting on a single MAC. Therefore, our results are equally well suited to small networks or large networks with structure and/or partitioning. Partitioning often arises due to the finite transmission range of the nodes, particularly in dense environments [30]. A predefined hierarchical structure, such as the tree network used in [32] also results in a highly structured network.

III. PROBLEM ANALYSIS

The general problem (5) is non-convex. We present a number of reformulations of the nonlinear constraints that can make the problem easier to solve in practice. The nonlinear rate constraints (5b) are convex in transmission powers p , but are not jointly convex in both transmission powers and distances χ . We will show that the nonlinear equality constraint (5f) may be substituted into the cost function, convexifying the cost. This, however, turns the previously simple thrust bound $F_{\min} \leq F_n(t)$ into a concave constraint, unless thrust bounds are relaxed. The absence of thrust bounds

arises when considering a fixed trajectory, or is a reasonable assumption if the speed range is sufficiently small. We finally give a number of special cases under which we may assure that all local optima are global optima.

Lemma 1. *For a communication link from U_n to U_m the received signal strength, defined as*

$$\Gamma(p_n, \chi_{mn}) \triangleq \eta_{mn}(\chi_{mn}, h_{mn})p_n = \frac{h_{mn}G_{mn}p_n}{\chi_{mn}^\alpha},$$

is quasiconcave.

Proof. Take $G_{mn}h_{mn} = 1$ for simplicity, and assume $\exists \pi_1 \triangleq (x_1, y_1), \pi_2 \triangleq (x_2, y_2) \in \mathbb{R}_+^2$ for which $\Gamma(\pi_i) \geq \beta, i \in \{1, 2\}$. Now consider the point $\lambda\pi_1 + (1 - \lambda)\pi_2, \lambda \in (0, 1)$,

$$\begin{aligned} \Gamma(\lambda\pi_1 + (1 - \lambda)\pi_2) &= \frac{\lambda x_1 + (1 - \lambda)x_2}{(\lambda y_1 + (1 - \lambda)y_2)^\alpha} \\ &\geq \beta \frac{\lambda y_1^\alpha + (1 - \lambda)y_2^\alpha}{(\lambda y_1 + (1 - \lambda)y_2)^\alpha} \geq \beta, \end{aligned}$$

which shows that the superlevel sets of $\Gamma(\cdot)$ are convex. The first step follows from $x_1 \geq \beta y_1^\alpha$ and $x_2 \geq \beta y_2^\alpha$. The second step follows from noting that $y \mapsto y^\alpha$ is convex on domain \mathbb{R}_+ , meaning that for $\lambda \in (0, 1), \lambda y_1^\alpha + (1 - \lambda)y_2^\alpha \geq (\lambda y_1 + (1 - \lambda)y_2)^\alpha$, and hence the fraction is ≥ 1 . \square

Corollary 1. *The rate constraints (5b) are convex when considering transmission power optimization over a fixed trajectory, but are not convex in the case of a free trajectory.*

Proof. For receiver U_m each capacity region constraint (5b) is of the form

$$\sum_{n \in S} r_n(t) - B_m \log_2 \left(1 + \frac{G\tilde{h}_n}{\sigma^2} \sum_{n \in S} \frac{p_n(t)}{\chi_{mn}(t)^\alpha} \right) \leq 0. \quad (7)$$

First, for a fixed trajectory (7) is only a function of r, p , while χ is fixed. The argument of the logarithm is linear in transmission powers. The function $\phi_1(x) \triangleq -\log(x)$ is convex, non-increasing. Since the composition of a convex, non-increasing function with a concave function is convex [33], and the linear combination of convex functions is also convex, (7) is convex in r, p . See [25] for further analysis.

When including the physical trajectory in the optimization, (7) is a function of r, p, q . The argument of the logarithm is now a sum of quasiconvex functions $\Gamma(\cdot)$ defined on separate domains. A linear combination of quasiconvex functions is not quasiconvex, unless all functions but one are strictly convex [34]. \square

Lemma 2. *For the general problem (5) of minimizing communication energy, the relaxation of (5c) to the convex constraint*

$$\chi_{mn}(t) \geq \|X_{mn}(t)\|^2 \quad (8)$$

does not change the solution.

Proof. Consider Y^* , the solution of (5), with (8) substituted instead of constraint (5c). Assume $\exists t \in \mathcal{T} : \chi_{mn}^*(t) > \|X_{mn}^*(t)\|^2$. If $p_{mn}^*(t) = 0$ then the optimal cost is not dependent on $\chi_{mn}^*(t)$. Otherwise $p_{mn}^*(t) > 0$ corresponds to a strictly positive rate $r_{mn}^*(t)$. Noting that rates are monotonically increasing in powers and monotonically decreasing in

distances, the same rate $r_{mn}^*(t)$ may still be achieved with a power $\tilde{p}_{mn}(t) < p_{mn}^*(t)$ if the corresponding $\tilde{\chi}_{mn}(t) > \|X_{mn}^*(t)\|^2$. Transmitting at power $\tilde{p}_{mn}(t)$ results in a strictly lower cost. Therefore Y^* cannot be a minimizer of (5), with (8) substituted instead of constraint (5c), unless

$$\chi_{mn}^*(t) = \|X_{mn}^*(t)\|^2, \forall t \in \mathcal{T}, \forall n, m \in \mathcal{N}, \forall p_{mn}^*(t) > 0.$$

This contradiction concludes the proof. \square

Consider χ_{mn} as a slack variable representing the squared distance between nodes U_m, U_n . Apart from its definition (5c), it appears only in the data rate constraints (5b), but not directly in the cost function or the dynamic constraints.

The posynomial objective function is also not convex over the whole of its domain and the logarithmic data rate term does not admit the use of geometric programming (GP) methods. However, convexification is possible by analysing the simplified problem in Lemma 3.

Lemma 3. *The following problem*

$$\min_{v_n, F_n} \int_0^T F_n(t)v_n(t)dt \quad (9a)$$

$$\text{s.t. } \forall t \in \mathcal{T}$$

$$F_n(t) - D(v_n(t)) = m_n \dot{v}_n(t) \quad (9b)$$

$$\underline{F} \leq F_n(t) \leq \bar{F} \quad (9c)$$

$$\underline{V} \leq v_n(t) \leq \bar{V} \quad (9d)$$

$$v_n(0) = v_{n,init}, \quad v_n(T) = v_{n,final} \quad (9e)$$

of minimizing just the propulsion energy of a single node U_n subject to thrust constraints, simple bounds, and initial and final conditions admits an equivalent convex form for all mappings D satisfying Assumption 1 and force bounds $(\underline{F}, \bar{F}) = (-\infty, \bar{F})$.

Proof. By noting that $F_n(t) = D(v_n(t)) + m_n \dot{v}_n(t)$, we move the equality into the cost function, rewriting the problem as

$$\min_{v_n} \phi(v_n) \text{ s.t. } (9c)-(9e),$$

where

$$\phi(v_n) \triangleq \underbrace{\int_0^T v_n(t)D(v_n(t))dt}_{\phi_1(v_n)} + \underbrace{m_n \int_0^T v_n(t)\dot{v}_n(t)dt}_{\phi_2(v_n)}.$$

We proceed by showing that both $\phi_1(\cdot)$ and $\phi_2(\cdot)$ are convex. Starting with the latter, by performing a change of variable, the analytic cost is derived by first noting that $\phi_2(v_n)$ is the change in kinetic energy

$$\phi_2(v_n) = m_n \int_{v_n(0)}^{v_n(T)} v dv = \frac{m_n}{2} (v_n^2(T) - v_n^2(0)),$$

which is a convex function of $v_n(T)$ subject to fixed initial conditions (9e); in fact, it is possible to drop the $v_n^2(0)$ term completely without affecting the minimizing argument. By Assumption 1, the mapping D is convex and continuous. Since integrals preserve convexity, the total cost function $\phi(\cdot)$ is convex.

Having removed the thrust F as a decision variable, satisfaction of input constraints would result in the set

$$\mathcal{V}_F \triangleq \{v_n \mid F_{\min} \leq D(v_n(t)) + m_n \dot{v}_n(t) \leq F_{\max}\}.$$

Even with $D(\cdot)$ convex on the admissible range of speeds, the lower bound represents a concave constraint not admissible within a convex optimization framework. Dropping the lower bounds on thrust results in a final convex formulation:

$$\begin{aligned} & \min_{v_n} \int_0^T v_n(t) D(v_n(t)) dt + \frac{m_n}{2} (v_n^2(T) - v_n^2(0)) \\ & \text{s.t. } \forall t \in \mathcal{T} \\ & \underline{V} \leq v_n \leq \bar{V} \\ & D(v_n(t)) + m_n \dot{v}_n(t) \leq \bar{F} \\ & v_n(0) = v_{n,\text{init}}, \quad v_n(T) = v_{n,\text{init}}. \end{aligned}$$

□

We now give two conditions for which all local solutions are global optima.

Theorem 1. *For fixed trajectories, the problem (5) is convex.*

Proof. For fixed trajectories χ , the decision variables are reduced to (p_n, r_n, s_n) , and constraints (5c), (5f) and (5j) may be omitted. The cost function is reduced to the sum of transmission powers. As such, convexity of the entire problem follows as a direct consequence of Corollary 1. □

For the special case of a single UAV link with fixed trajectories this problem becomes one of power allocation over known time-varying channels, which has been addressed in various forms in the literature (e.g. [16, Chapter 5]). An example of this, with further analysis, is given in Section IV-A. In the multi-user setting for fading channels, [25] proposed solving this special case with a greedy algorithm for optimal rate and power allocation over MAC.

Lemma 4. *Consider the monotonically non-increasing function $h : \mathbb{R} \rightarrow \mathbb{R}$ and the quasiconcave function $g : \mathcal{C} \subset \mathbb{R}^n \rightarrow \mathbb{R}$. The composition $h \circ g$ is quasiconvex.*

Proof. From the quasiconcavity of g ,

$$\min\{g(x), g(y)\} \leq g(\lambda x + (1 - \lambda)y), \forall \lambda \in (0, 1).$$

Since h is monotonically non-increasing, $a \leq b \Leftrightarrow h(a) \geq h(b)$, hence

$$h(\min\{g(x), g(y)\}) \geq h(g(\lambda x + (1 - \lambda)y)).$$

Noting that,

$$h(\min\{g(x), g(y)\}) = \max\{h(g(x)), h(g(y))\},$$

we may conclude

$$\max\{h(g(x)), h(g(y))\} \geq h(g(\lambda x + (1 - \lambda)y)),$$

and hence the quasiconvexity of $h \circ g$. □

In [33, Chapter 3.4.4] a similar statement as above is presented, but for composition of quasiconvex and non-decreasing functions.

Theorem 2. *Consider a set of UAVs $U_n, n \in \mathcal{N}$. Assume that communication is restricted to multi-hop transmissions, where node U_n transmits only to $U_{n+1}, \forall n \neq N$, reducing the communication network to single access channels. The problem of joint trajectory and transmission power optimization in order to sustain a constant minimum communication rate \bar{r} is*

$$\min_{Y_n, n \in \mathcal{N}} \sum_{n=1}^N \int_0^T p_n(t) + v_n(t) F_n(t) dt \quad (11a)$$

$$\text{s.t. } \forall n \in \mathcal{N}, \forall m \in \mathcal{N} \setminus \{N\}, \forall t \in \mathcal{T},$$

$$-B_{(m+1)} \log_2 \left(1 + \frac{G_{m(m+1)}}{\sigma^2} \left(\frac{p_m(t)}{\chi_{m(m+1)}(t)^\alpha} \right) \right) \leq -r, \quad (11b)$$

$$\chi_{m(m+1)}(t) = \|X_{m(m+1)}(t)\|^2, \quad (11c)$$

$$q_n(0) = Q_{n,\text{init}}, \quad q_n(T) = Q_{n,\text{final}}, \quad (11d)$$

$$v_n(0) = v_{n,\text{init}}, \quad (11e)$$

$$F_n(t) = m_1 \dot{v}_n(t) + \Omega(v_n(t)), \quad (11f)$$

$$\dot{q}_n(t) = \Upsilon_n v_n(t). \quad (11g)$$

$$Y_{n,\text{min}} \leq Y_n(t) \leq Y_{n,\text{max}}. \quad (11h)$$

In the absence of constraints on thrust, all local optima of the above problem are global optima.

Proof. Using Lemmas 2 and 3, problem (11) is equivalent to

$$\min_{p,r,s,q,v} \sum_{n=1}^N \left[\int_0^T p_n(t) + v_n(t) \Omega(v_n(t)) dt + \frac{m_n}{2} v_n^2(T) \right]$$

$$\text{s.t. } \forall n \in \mathcal{N}, \forall m \in \mathcal{N} \setminus \{N\}, \forall t \in \mathcal{T},$$

$$(11b), (8), (11d), (11e), (11g), \tilde{Y}_{n,\text{min}} \leq \tilde{Y}_n(t) \leq \tilde{Y}_{n,\text{max}}$$

where $\tilde{Y}_n(t) \triangleq (p_n(t), r_n(t), s_n(t), q_n(t), v_n(t))$, and the bounds $\tilde{Y}_{n,\text{min}}$, and $\tilde{Y}_{n,\text{max}}$ are similarly changed. The cost function and all the constraints, apart from (11b), are convex. However, the function

$$\xi(p_m, \chi_{m(m+1)}) \triangleq -\log \left(1 + \sigma^{-2} \Gamma(p_m, \chi_{m(m+1)}) \right)$$

was shown to be quasiconvex. As noted in Lemma 1, $\Gamma(\cdot)$ is quasiconcave for all $\alpha > 1$. From Lemma 4, the composition of a monotonically nonincreasing function with a quasiconcave function is quasiconvex. Therefore $\xi(\cdot)$ is quasiconvex. A direct implication is that the set

$$\mathcal{R}_m \triangleq \{(p_m, \chi_{m(m+1)}) \mid \xi(p_m, \chi_{m(m+1)}) \leq r\}$$

is convex for each m . Since all the other constraints are linear, the constraint set is an intersection of half spaces with convex sets \mathcal{R}_m , which is convex. Minimizing a convex cost over a convex set implies that all local optima are global optima. □

IV. SPECIAL CASES

The following analysis is for basic single-hop network topologies, with example settings depicted in blue in Figure 1. The use of nonlinear models render the general problem (5) non-convex, with non-trivial solutions. Here we consider general AWGN channels. We also present particular cases of the problem, for which (known) analytic solutions exist. Our

formulation allows for new insights into these special cases. In Sections IV-A and IV-B, respectively, we focus on single and multiple access networks, with supporting numerical results presented in Section IV-C. Parameters used in all the simulations are defined in Table I, where the chosen UAV speed range is consistent with [5].

A. Single UAV

Consider a UAV U_{a1} moving from $(Q_{\text{init}}, 0, a_{a1})$ to $(Q_{\text{final}}, 0, a_{a1})$, passing directly over a stationary AP U_0 positioned at $(0, 0, 0)$. Over time T , U_{a1} is required to offload D_{a1} bits of data. We may simplify this problem by assuming the velocity profile of U_{a1} is fixed and optimizing only over transmission policies. The predefined trajectory results in time-varying channel gains $\eta_{01}(t)$ which are fixed a priori. The optimal transmission scheme is then characterized by a water-filling solution [35], which is a general term for equilization strategies used for power allocation in communication channels. Water-filling allows us to cast the infinite-dimensional OCP as a single-dimensional problem. A water-filling solution for *rate maximization* may be found in [35]. In the following new result, we instead present a proof for *power minimization*. Variable subscripts are dropped for notational simplicity.

Proposition 1. *For a mobile transmitter with a predefined trajectory relative to a stationary receiver, over time interval \mathcal{T} , the minimum transmission energy required to communicate D bits of data is found by solving*

$$p^* \in \arg \min_p \int_0^T p(t) dt \quad (13a)$$

$$\text{s.t. } \int_0^T \ln \left(1 + \frac{\eta(t)p(t)}{\sigma^2} \right) dt = D, \quad (13b)$$

$$0 \leq p(t) \leq P_{\max}, \quad \forall t \in \mathcal{T}, \quad (13c)$$

which takes the form

$$p^*(t) = \min \{ P_{\max}, \max \{ 0, (\zeta - \sigma^2/\eta(t)) \} \},$$

where scalar ζ is a dual variable and $\eta(t) \triangleq \eta(\chi(t), h)$ is the time-varying channel gain due to fixed source trajectory.

Proof. Isolate variables $p(t)$ by rewriting (13b) as

$$\int_0^T \ln \left(\frac{\sigma^2}{\eta(t)} + p(t) \right) dt = \tilde{D},$$

$$\tilde{D} = D - \int_0^T \ln \left(\frac{\sigma^2}{\eta(t)} \right) dt.$$

The Lagrangian of (13) is

$$L(p, \zeta, \rho, \gamma) = \int_0^T (-\rho(t)p(t) + \gamma(t)(p(t) - P_{\max})) dt$$

$$- \zeta \left(\int_0^T \log_2 \left(\frac{\sigma^2}{\eta(t)} + p(t) \right) dt - \tilde{D} \right),$$

TABLE I: Common model and simulation parameters.

σ^2	B	M	P_{\max}	α	T	$(\underline{V}_n, \overline{V}_n)$	m
[W]	[Hz]	[GB]	[W]	[-]	[min]	[m/s]	[kg]
10^{-10}	10^5	1	100	1.5	20	(12, 28)	3

where dual variables $\rho(t), \gamma(t), \zeta$ correspond to the lower and upper bounds, and the integral data constraint. First-order optimality conditions result in the following solution,

$$p^*(t) = \begin{cases} 0, & \text{if } \zeta \leq \frac{\sigma^2}{\eta(t)}, \\ P_{\max}, & \text{if } \zeta \geq \left(\frac{\sigma^2}{\eta(t)} + P_{\max} \right), \\ \left(\zeta - \frac{\sigma^2}{\eta(t)} \right), & \text{otherwise.} \end{cases}$$

□

We may interpret $\sigma^2/\eta(t)$ as the effective noise power at time t after normalizing with the channel gain. Intuitively, there exists a constant received power level $\sigma^2 + \eta(t)p(t)$ over \mathcal{T} for which D bits of data is communicated using minimal transmission energy. A binary search may be used to find ζ .

The above result does not readily extend to when the source/receiver trajectory is not predetermined because the channel gains are no longer fixed. However, the transmission scheme of the jointly optimal solution to problem (5) will be a water-filling solution of the channel gains corresponding to the optimal trajectory. In some cases we may seek to determine the UAV trajectory $v(t)$ that maximizes data transfer, subject to peak power constraints and mobility dynamics. That is, we do not constrain the total energy consumption in order to characterise the maximum amount of data offloadable from the UAV.

Proposition 2. *Consider a single-dimensional space, with a stationary receiver located at the origin and a mobile transmitter moving along a linear path from $0 < Q_{\text{init}} < Q_{\text{final}}$ over time \mathcal{T} . Without thrust constraints the data transfer $\int_{\mathcal{T}} r(t) dt$ is maximized for the transmitter speed profile,*

$$v^*(t) = \begin{cases} \underline{V}, & \forall t \in [0, t_1] \\ \overline{V}, & \forall t \in [t_1, T]. \end{cases} \quad (14)$$

Proof. For maximum data transfer, we set $p(t) = P_{\max}, \forall t \in \mathcal{T}$. A trajectory is feasible if the node's speed satisfies the box constraints of set \mathcal{V} and the node traverses the required distance, that is,

$$\int_0^T v(t) dt = Q_{\text{final}} - Q_{\text{init}}, \quad v(t) \in [\underline{V}, \overline{V}], \forall t \in \mathcal{T}.$$

For a feasible problem we have $\underline{V}T \leq Q_{\text{final}} - Q_{\text{init}} \leq \overline{V}T$. The single user capacity is a strictly decreasing function of the distance $\chi(\cdot) = q(\cdot)$ between transmitter and receiver. Furthermore, because $Q_{\text{final}} > Q_{\text{init}}$ and $\underline{V} > 0$, $\chi(t)$ is strictly decreasing in t . Due to the monotonicity of the capacity function, a sufficient condition for optimality of the speed profile $v^*(\cdot)$, and correspondingly optimal distance $\chi^*(\cdot)$ is that

$$\chi^*(t) \leq \chi(t) = \int_0^t v(\tau) d\tau, \forall t \in \mathcal{T}, \quad (15)$$

where $\chi(\cdot)$ is any continuous trajectory corresponding to a feasible speed $v(\cdot)$. Clearly, the position

$$\chi^*(t) = Q_{\text{init}} + \underline{V}t \leq \chi(t)$$

satisfies (15), but is only feasible if it is still possible to reach the final destination by time T , i.e.

$$\chi^*(t) + \bar{V}(T - t) \geq Q_{\text{final}}.$$

We use t_1 to denote the time when this is satisfied with equality. From position $\chi^*(t_1)$ at time t_1 the *only* way to satisfy boundary conditions is to move at maximum speed \bar{V} for remaining time $T - t_1$. Since $\chi^*(t_1) \leq \chi(t_1)$, and there exists only a single feasible speed profile that satisfies boundary conditions over $(t_1, T]$, the trajectory

$$\chi^*(t) = \begin{cases} Q_{\text{init}} + \underline{V}t, & \text{if } t \in [0, t_1), \\ Q_{\text{init}} + \underline{V}t_1 + \bar{V}(t - t_1), & \text{if } t \in [t_1, T], \end{cases}$$

corresponding to (14) must satisfy (15) $\forall t \in \mathcal{T}$, where

$$t_1 \triangleq ((Q_{\text{final}} - Q_{\text{init}}) - \bar{V}T) (\underline{V} - \bar{V})^{-1}.$$

□

For brevity we have only considered a UAV trajectory moving away from the source. By similar arguments we may see that in the case of $Q_{\text{init}} < 0 < Q_{\text{final}}$ (assuming non-zero UAV altitude and source located at origin) the optimal speed profile would be piecewise constant with

$$v^*(t) = \bar{V} \forall t \in [0, t_1) \cup (t_2, T]; \quad \underline{V} \forall t \in [t_1, t_2].$$

If the UAV were able to hover (e.g. rotor-crafts) then the data-maximizing trajectory would require the UAV to hover at the point along its trajectory closest to the receiver – analogous to the hover-fly-hover protocol [12].

B. Two UAVs

Consider the transmission energy problem for UAVs U_{a1}, U_{a2} travelling along predefined trajectories (e.g., the parallel trajectories shown in Figure 1) relative to stationary U_0 . We allocate no bandwidth to U_{a1}, U_{a2} for receiving transmission. The result is a single MAC with $N = 2$ transmitters U_{a1}, U_{a2} and receiver U_0 . The capacity region $\mathcal{C}_2(\chi, p, h)$ is the set of non-negative rate tuples (r_{a1}, r_{a2}) satisfying

$$0 \leq r_{a1} \leq B_0 \log_2 \left(1 + \frac{\eta(\chi_{10}, h_{a1})p_{a1}}{\sigma^2} \right) \quad (16a)$$

$$0 \leq r_{a2} \leq B_0 \log_2 \left(1 + \frac{\eta(\chi_{20}, h_{a2})p_{a2}}{\sigma^2} \right) \quad (16b)$$

$$r_{a1} + r_{a2} \leq B_0 \log_2 \left(1 + \frac{\eta(\chi_{10}, h_{a1})p_{a1} + \eta(\chi_{20}, h_{a2})p_{a2}}{\sigma^2} \right) \quad (16c)$$

for all $(p_{a1}, p_{a2}) \in \mathcal{P}^2$. The first two are single-user bounds for each source. Information independence between U_{a1}, U_{a2} leads to the final constraint that the sum rate may not exceed the point-to-point capacity with full cooperation. For transmission powers (p_{a1}, p_{a2}) the set of achievable rates is the pentagon in Figure 2. The rate tuple at vertex $R^{(1)}$ is achieved if the signal from U_{a2} is decoded entirely before U_{a1} . For a reversed decoding order the network operates at $R^{(2)}$.

With reference to Figure 2, the sum rate $r_{a1} + r_{a2}$ is maximized at any point on segment L_3 . Therefore, for any given power tuple (p_{a1}, p_{a2}) , the optimal rate tuple will lie on

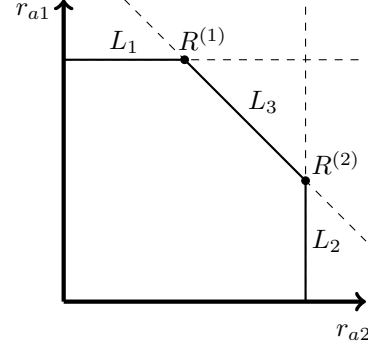


Figure 2: Capacity region for a given power policy across two parallel channels. Corner rates labelled as $R^{(1)} = (r_{a1}^{(1)}, r_{a2}^{(1)})$ and $R^{(2)} = (r_{a1}^{(2)}, r_{a2}^{(2)})$. Line segments labelled as L_1, L_2, L_3 .

segment L_3 . This is formalized in Proposition 3. Equivalently we may construct any optimal rate pair $R^{(*)} = (r_{a1}^{(*)}, r_{a2}^{(*)})$ as the weighted sum

$$R^{(*)} = \varphi \cdot R^{(1)} + (1 - \varphi) \cdot R^{(2)},$$

for $\varphi \in [0, 1]$.

The number of capacity region constraints grow exponentially with the number of MAC users. An important question is whether we can use the structure of the capacity region to simplify the problem statement. For the $N = 2$ user case we observed that optimal rate points lie on the boundary L_3 , which implies that the number of *active* constraints at an optimal point scales at most linearly with the number of transmitters. This observation is formalized in the following lemma.

Proposition 3. Consider a MAC with $N = 2$ users U_{a1}, U_{a2} located at distances χ_{a1}, χ_{a2} . For any arbitrary non-trivial rate pair (r_{a1}, r_{a2}) the minimum power is achieved by first decoding the user with the better channel state, and subtracting this decoded signal from the remaining signal.

Proof. To emphasise that we are manipulating the power pairs (p_{a1}, p_{a2}) to achieve a particular rate pair $R^{(*)}$, we rearrange (16) to isolate transmission powers as

$$\sigma^2 \left(2^{\frac{r_{a1}}{B_0}} - 1 \right) \leq \chi_{a1}^{-\alpha} p_{a1}, \quad (17a)$$

$$\sigma^2 \left(2^{\frac{r_{a2}}{B_0}} - 1 \right) \leq \chi_{a2}^{-\alpha} p_{a2}, \quad (17b)$$

$$\underbrace{\sigma^2 \left(2^{\frac{r_{a1} + r_{a2}}{B_0}} - 1 \right)}_{\Lambda} \leq \chi_{a1}^{-\alpha} p_{a1} + \chi_{a2}^{-\alpha} p_{a2}. \quad (17c)$$

Say that AN arbitrary non-trivial rate pair $R^{(*)} = (r_{a1}, r_{a2})$ is achieved with transmission power pair (p_{a1}, p_{a2}) . Due to the superlinearity of the $\exp(\cdot)$ function, (17c) prevents both (17a) and (17b) from being simultaneously satisfied with equality.

Consider the case in which (17c) holds with strict inequality. In this case, (p_{a1}, p_{a2}) cannot be optimal in the sense of minimising $p_{a1} + p_{a2}$ because one or both of (p_{a1}, p_{a2}) may be reduced while still satisfying (17). Therefore any optimal power allocation must satisfy (17c) with equality.

TABLE II: Transmission energy ϵ_T and propulsion energy ϵ_P usage of nodes U_{a1}, U_{a2} for simulations analysed in Section IV.

Simulation	U_{a1} (kJ)		U_{a2} (kJ)	
	ϵ_T	ϵ_P	ϵ_T	ϵ_P
$N = 1$ fixed ($D_{a1} = 45$ MB)	69.5	143.9	—	—
$N = 1$ free ($D_{a1} = 65$ MB)	102.9	168.9	—	—
$N = 2$ fixed ($D_{a1}, D_{a2} = 22$ MB)	43.6	143.9	22.2	143.9

Now, given that (17c) holds with equality, we rearrange to isolate p_{a1} , resulting in

$$p_{a1} = \frac{\Lambda}{\chi_{a1}^{-\alpha}} - \left(\frac{\chi_{a1}}{\chi_{a2}} \right)^\alpha p_{a2}. \quad (18)$$

If $\chi_{a1} > \chi_{a2}$, then the sum power may be reduced by increasing p_{a2} , while increasing p_{a1} to satisfy (18), until constraint (17a) holds with equality. Otherwise, the sum power may be reduced by increasing p_{a1} and reducing p_{a2} until constraint (17b) holds with equality. With reference to Figure 2, these cases are equivalent to operating at $R^{(*)} = R^{(1)}$ or $R^{(*)} = R^{(2)}$, respectively, achieved when $\varphi \in \{0, 1\}$. \square

Sum power-optimal decoding order leaves the user with the worst channel until last, independent of the data rates. Proposition 3 shows that, for fixed trajectories, the set of active rate constraints may be determined offline.

C. Numerical Results

Continuous-time problems are transcribed using ICLOCS2² [31] and numerically solved using the open source primal dual Interior Point solver Ipopt [37]. ICLOCS2 allows for rate constraints to be directly implemented on the discretized problem mesh. This prevents singular arcs and improves computational efficiency [38]. We use this feature to place derivative constraints (5h) on acceleration. Energy usage for simulations discussed in this section may be found in Table II.

We first present results for the single user case with fixed trajectory (Section IV-A). The solution is shown in Figure 3 for fixed UAV velocity profile

$$v_{a1}(t) = v_{\text{avg}} = \frac{1}{T}(Q_{a1, \text{final}} - Q_{a1, \text{initial}}).$$

Due to strict convexity of the drag function (4), this constant velocity profile uses minimum propulsion energy. Agreeing with Proposition 1, an inverse relationship between $p_{a1}(t)$ and the effective noise $\sigma^2/\eta_{a1,0}(t)$ is shown, where ζ coincides with the peak transmission power. Here U_{a1} was initialized with $D = 50$ MB. We observe that U_{a1} transmits only within a certain proximity of the static destination node, and more power is allocated for transmission when it is closer to the destination.

If instead we allow U_{a1} to have a free trajectory then the jointly optimal transmission and mobility profiles of U_{a1}

²Transcription involves conversion of the original continuous time optimal control problem into a nonlinear program [36]. Various transcription methods exist, with the appropriate one often depending on characteristics of the problem. ICLOCS2 supports various different transcription methods.

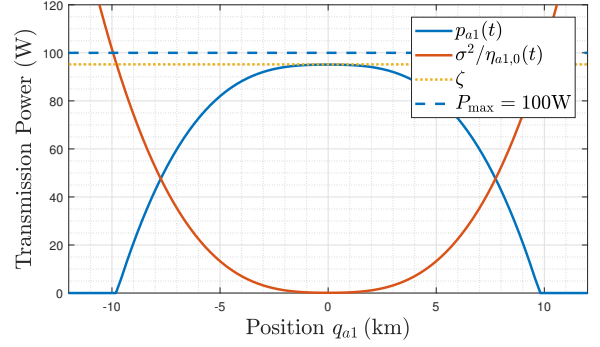
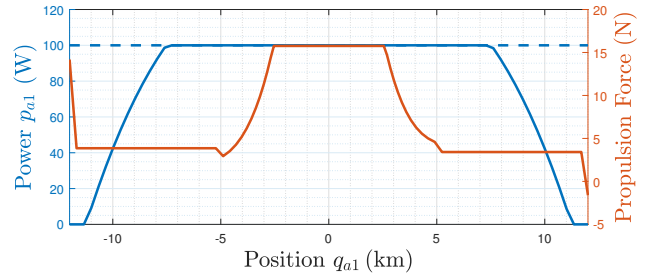


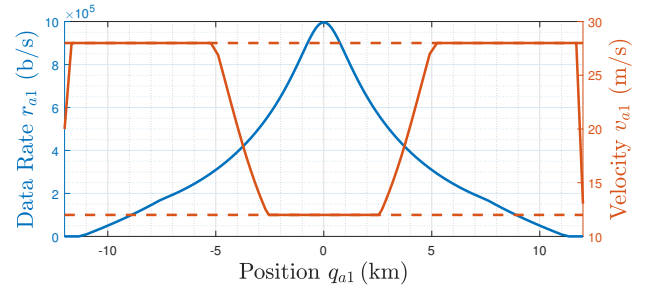
Figure 3: Optimal power and rate allocation for a single-node U_{a1} at constant speed is characterized entirely by the scalar ζ .

generated by problem (5) are shown in Figure 4 for a greater starting load of $D = 65$ MB. U_{a1} moves at velocity \bar{V} when it is further from the transmitter, but then expends energy to slow down to \underline{V} when it is close to the AP in order to maintain a better channel for a longer duration. During this time the UAV is transmitting at peak power in order to opportunistically exploit the favourable channel gain. Considering the insights of Lemma 2, we may correctly surmise that 65 MB is close to the network capacity.

Simulation results for the two node fixed trajectory problem (Section IV-B) are shown in Figure 5, where U_{a1}, U_{a2} are initialized with data $D_{a1} = D_{a2} = 22$ MB and travel at fixed speeds of 72 km/h. The distances $\chi_{01}(t) < \chi_{02}(t), \forall t \in \mathcal{T}$ are such that U_{a1} experiences a more favourable channel at each time instance. The transmission profile of U_{a1} bears strong resemblance to the single user case. Interestingly,

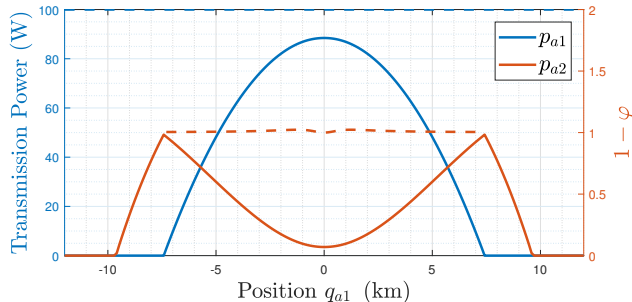


(a) Optimal transmission power and thrust profile of U_{a1} .

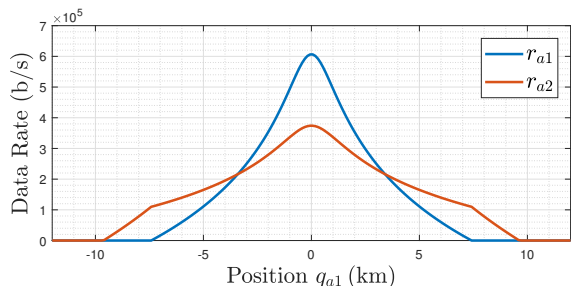


(b) Associated achieved data rate and velocity profile of U_{a1} .

Figure 4: Single-node problem. Dashed lines indicate bounds on respective variables corresponding to $\underline{Y}_n \leq Y_n(t) \leq \bar{Y}_n$.



(a) Transmit powers of nodes U_{a1} and U_{a2} , and the associated decoding order r at the receiving AP.



(b) Associated transmission rates achieved by nodes U_{a1} and U_{a2} .

Figure 5: Two-node transmission power problem.

when both U_{a1}, U_{a2} are transmitting, U_{a2} is able to increase transmission rate while decreasing transmission power. As shown in Table II, this policy actually results in U_{a2} using less transmission energy than U_{a1} . We may explain this with reference to Proposition 3. The mapping $t \mapsto \varphi(t)$ may be a time-varying priority, and is only uniquely defined when $p_n(t) > 0, n \in \{1, 2\}$. If we calculate $\varphi(\cdot)$ from the optimal powers and rates shown in Figure 5, we find that $\varphi(t) = 0, \forall t \in \{t \in \mathcal{T} \mid p_n(t) > 0, n \in \{1, 2\}\}$. In words, when both nodes are transmitting, the optimal policy in terms of total energy is to give decoding priority to the node with the worst channel (U_{a2}). Another consequence of Proposition 3 is that since $\chi_{01}(t) < \chi_{02}(t), \forall t \in \mathcal{T}$, we need not specify bound (16a) to obtain the optimal trajectory in Figure 5.

V. RELAY-ASSISTED INTERNET-OF-THINGS (IOT) NETWORK

The following examples are representative of a relay-assisted wireless sensor network. We consider the geometry shown in Figure 1, where a set of terrestrial source nodes $U_{gn}, n \in \{1, \dots, N-1\}$, are geographically isolated from AP U_0 and must offload their data. We first consider the relay to be an ideal sink and look at the energy savings available through joint optimization of the relay's trajectory with the source's transmissions. We then extend these simulations by assuming the UAV U_N has a finite data buffer; and hence, must relay data to U_0 . Later in this section we will include uncertainty by considering communication over slow fading channels, and in doing so introduce successful decoding conditions.

TABLE III: Transmission energy of source i , ($\epsilon_{gi}, i \in \{1, 2\}$) and UAV propulsion energy (ϵ_{a1}) for UAV uplink under different schemes.

	Separate BW		Shared BW (MAC)	
	$v = v_{\text{avg}}$	$v = v^*$	$v = v_{\text{avg}}$	$v = v^*$
ϵ_{a1}	NA	1	0.311	0.201
ϵ_{g1}	NA	1	0.381	0.257
ϵ_{g2}	NA	1	0.861	0.885

A. Open-loop Energy Savings

We perform open-loop simulations assuming ideal AWGN channels to compare the potential energy savings. Suppose there exist source nodes U_{g1}, U_{g2} that must offload all their data to a receiving UAV U_{a1} . The UAV operates as an ideal sink with no memory constraints, $M = D_{a1} = \infty$. Sources are initialized with a starting data load $D_{g1} = D_{g2} = 25$ MB. Communication occurs over a two-user MAC, where the set of achievable rate tuples is upper bounded by three functions of the form (16). This is the first result to combine mobility with transmission over a MAC.

We construct comparative schemes using the following physical network constraints. Firstly, resources may be partitioned such that there is no inter-user interference. Therefore U_{g1}, U_{g2} transmit on orthogonal channels of designated bandwidth³ $B_{g1} = B_{g2} = B_{a1}/2$. Partitioning B is computationally simpler, since the number of constraints scale linearly (not exponentially) with the number of sources. Secondly, transmission policies may be optimized subject to a fixed UAV trajectory. In this case we assume that U_{a1} moves at constant speed v_{avg} using minimal propulsion energy. Combinations of these constraints results in four possible protocols.

Table III shows a comparison of the total energy usage ϵ_C , equivalent to the cost function (5a), and the transmission energy $\epsilon_{g1}, \epsilon_{g2}$ used by the source nodes in each scheme. All energies are given as a ratio of the worst case feasible scenario. In the simplest case, where U_{g1}, U_{g2} transmit over orthogonal channels and U_{a1} moves at a fixed speed, the optimal transmission policy of each node is a water-filling solution, determined by a single water-filling parameter [16]. This reduces the infinite-dimensional search space of the original OCP to a single dimension. However, for the given starting data load, the problem is infeasible under these conditions.

Generating a solution by solving (5) results in a 36% total energy savings when compared with joint optimization over single access channels, while sources U_{g1}, U_{g2} respectively use 80% and 75% less transmission energy. Although there is not significant network level energy savings for the MAC uplink under different speed regimes, both U_{g1}, U_{g2} save 36% and 33% transmission energy, respectively, by allowing the relay to vary speed. This may be of particular importance in remote sensing applications, where source nodes may have strict energy requirements or perform energy harvesting [39].

³Results may be improved through optimally partitioning the bandwidth, which we do not do. Due to the identical starting loads, and similar channel gains, it is expected that equal bandwidth allocation is close to optimal.

B. Closed-Loop Simulation

For a closed-loop simulation, an NMPC control policy is generated by solving (5) at each computation interval $t_c = 10$ s, subject to initial conditions set by measured data. We consider the geometry illustrated in green in Figure 1, where sources U_{g1}, U_{g2} are initialised with $D_{g1} = D_{g2} = 11$ MB and U_{a1} has a finite memory constraint of $M = 1.5D_{g1}$. All data must be relayed to the AP U_0 by time T . The finite time nature of the experiment motivates the use of a decreasing horizon strategy, where the final time is constant and the horizon length is reduced at each t_c . The NMPC problem is solved centrally, with full state information. In practice, position and velocity information can be obtained from GPS and IMU data.

Typically data is encoded and sent in discrete codewords over packet intervals $t_p \ll t_c$. At each computation interval the complete information at each node is encoded at rates determined by (5). We assume a repeat request (ARQ) protocol. Transmitters get feedback through 1-bit acknowledgement (ACK/NAK) signals. Buffers are only updated with successfully decoded information. Information in an unsuccessfully decoded codeword is retransmitted at a later time.

Here we assume slow fading channels, where the channel realizations are random but remain constant over t_p . Therefore, at the beginning of each interval the channel state is modelled as a new realization of the random channel variable. We therefore formulate (5) with ϵ -outage capacity constraints, ensuring the control policy is robust to channel realizations. In the following we consider the MAC channel over a single codeword interval, dropping time dependency in notation. For actual realization \tilde{h}_n , channel outage — where the codeword is not successfully decoded — occurs because one or more of the received powers $\tilde{\beta}_n \triangleq \eta(\chi_{rn}, \tilde{h}_n)p_n$ was smaller than predicted and cannot support rate r_n . The decoder may perform joint decoding of received signals, or decode a subset of received signals, treating others as interference. Precisely, for an N -user MAC, information transmitted from users in $S \subseteq \mathcal{N}$ is successfully decoded if

$$r \in \mathcal{D} \triangleq \bigcup_{S \subset \mathcal{N}} \left\{ r > 0 \mid \sum_{m \in \mathcal{M}} r_m - B \log_2 \left(1 + \underbrace{\frac{\sum_{n \in \mathcal{M}} \tilde{\beta}_n}{\sigma^2 + \sum_{s \in S'} \tilde{\beta}_s}}_{\text{SNIR}} \right) \leq 0, \forall \mathcal{M} \subset S \right\}$$

where $S' \triangleq \mathcal{N} \setminus S$ is the set of users not decoded, treated only as interference. Figure 6 shows this region for an $N = 2$ user MAC. Since the rate tuple generated by (5) is always on the boundary of the capacity region, we may determine if $r \in \mathcal{D}$ just by considering actual and predicted received powers. If the actual SNIR is at least as large as the predicted SNIR, i.e.

$$\frac{\sum_{m \in \mathcal{M}} \beta_m}{1 + \sum_{j \in S'} \beta_j} \geq \frac{\sum_{m \in \mathcal{M}} \tilde{\beta}_m}{1 + \sum_{j \in S'} \tilde{\beta}_j}, \forall \mathcal{M} \subseteq S,$$

where $\beta_M \triangleq \eta(\chi_{rm}, F_h^{-1}(1 - \epsilon))p_m$, then users $U_i, i \in \mathcal{M}$ can be decoded. For a single user channel, this simplifies to $\beta_{a1} \geq \tilde{\beta}_{a1}$.

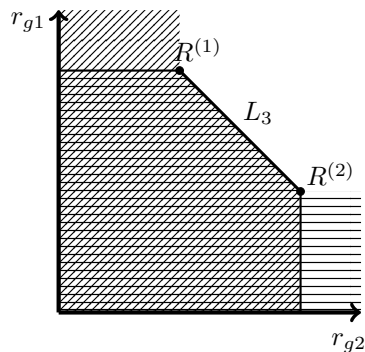


Figure 6: Two user decoding region. Region shaded by horizontal lines contains rates decodable from U_{g1} . Region shaded by vertical lines contains rates decodable from U_{g2} .

UAVs are advantageous in communication networks due to line of sight (LoS) links. Multipath scattering may still occur, such as off of objects near ground nodes or flight surfaces of the UAV. Rician fading is suitable for modelling received signal strength in channels with strong LoS components [40]. For each channel used, ν is a vector of random variables drawn from a Rice distribution characterized by K-factor κ , defined as the ratio of received signal power in the LoS path to the power received from scattered paths. If $\kappa = \infty$ there is no fading, and the model reduces to AWGN [40]. Similarly, for terrestrial applications with no LoS, $\kappa = 0$ results in the commonly-used Rayleigh model [40]. The cumulative distribution $\Gamma(\cdot)$ of a Rician channel is a Marcum Q-function of order 1. In our simulations we set $\kappa = 10$, and assume that the fading processes of different users are independent and identically distributed,

$$v_{nm} \sim \text{Rice} \left(\sqrt{\kappa(\kappa + 1)^{-1}}, \sqrt{(2(\kappa + 1))^{-1}} \right),$$

for each fading instance and each pair of nodes n, m .

The UAV may be disturbed by wind during flight. We model wind entering the first derivative [23] such that ground speed \dot{q} is the sum of air speed \dot{v} and wind speed \dot{w} . To account for this, the state is augmented with disturbance variable $\delta(t)$,

$$\dot{\delta}(t) = 0, \forall t \in \mathcal{T}, \delta(0) = w_{\text{meas}}$$

and redefined position dynamics

$$\dot{q}(t) \triangleq \Upsilon v(t) - \delta(t).$$

With full state information the estimate \hat{w}_{meas} is calculated through a moving average filter. For simulation, we let $\dot{w} = -6$ m/s.

The finite time problem may be infeasible due to channel outages and wind disturbances. In this case we switch to a variable terminal time for the last few iterations (the convergence analysis of the variable horizon scheme could be a topic of future work). Simulations are performed for $\Gamma^{-1}(1 - \epsilon) \approx 0.2$, with results shown in Figures 7–8. In this simulation, as in Figure 1, two ground nodes U_{g1}, U_{g2} are relaying data to a single access point via UAV U_{a1} . Figure 7a shows the mobility dynamics of the UAV, where a velocity constraint

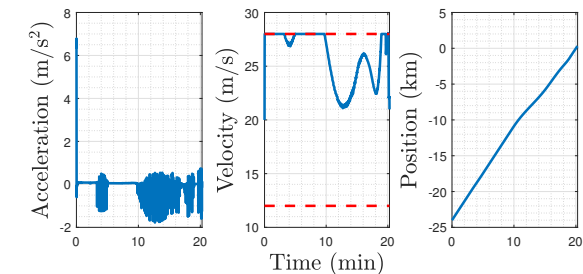
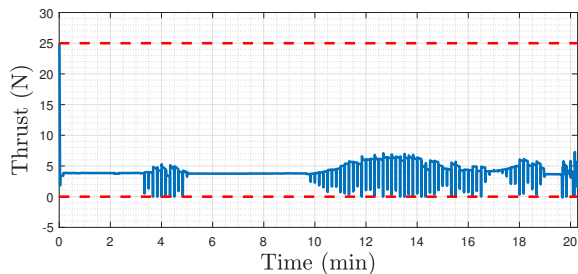
(a) U_{a1} acceleration, velocity and displacement profiles.(b) U_{a1} thrust profile.

Figure 7: Mobility related state/input trajectories (solid lines) for U_{a1} during relay simulation. Dashed lines show constraints.

becomes active as the UAV slows down to offload collected data to the AP. The extreme change in velocity results from the UAV memory s_{a1} approaching capacity. Figure 7b shows the thrust required to maintain altitude during this maneuver. Since $C_{D2} \gg C_{D1}$ in (4), a wind speed of $\dot{w} = -6$ beneficially slows down the UAV, reducing the minimum energy by $\approx 31\%$ compared to a wind speed of $\dot{w} = 6$.

Commanded rates over t_c are strict upper bounds on achievable information transfer because, even for favourable channel realizations, data will not be transferred faster than predicted. Figures 8a–8b show data interchange between $U_i, i \in \{0, g1, g2, a1\}$ in terms of the storage memory and achieved rates. Figure 8c shows the associated transmission power profile. Maximum power constraints are active while the UAV's buffer is close to capacity, during which the incoming and outgoing data from U_{a1} are similar. Due to the nonzero probability of outage, we cannot guarantee all data will be offloaded in \mathcal{T} , or indeed in any finite time. In case (5) becomes infeasible, which often happens as $t \rightarrow \sup \mathcal{T}$ due to the hard terminal data constraint (5e), we allow for a variable terminal time. In practice we see that an average of 4.9 kB of the initial 22 MB remains on $s_{a1}(T)$, which takes another 1.55 s to offload to U_0 , an increase in T of approximately 1%.

VI. CONCLUSIONS AND FUTURE WORK

We have formulated nonlinear dynamic models for transmission and mobility in UAV-enabled networks. We have considered both a Shannon capacity formulation for static AWGN channels and an outage capacity formulation for time-varying slow fading channels. Building upon these models, we have presented a general optimization framework for joint

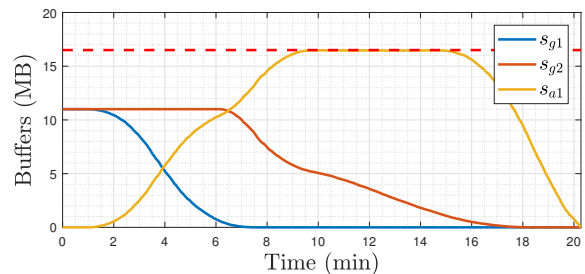
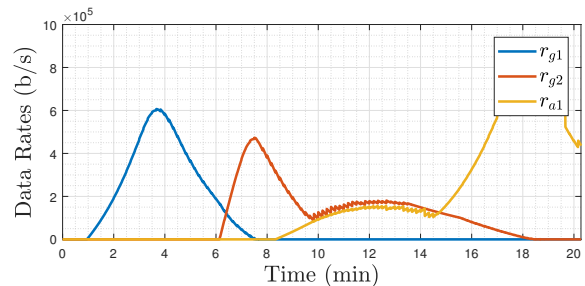
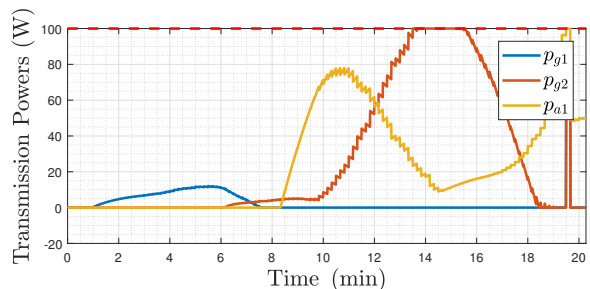
(a) Data storage buffers of U_{g1}, U_{g2}, U_{a1} .(b) Transmission data rates of U_{g1}, U_{g2}, U_{a1} .(c) Allocated transmission powers of U_{g1}, U_{g2}, U_{a1} .

Figure 8: Transmission related state/input trajectories (solid lines) for nodes U_{g1}, U_{g2}, U_{a1} during UAV relay simulation. Dashed lines show hard constraints.

control of propulsion and transmission in mobile communication networks. Special cases where the OCP may either be solved to global optimality or relates to existing solutions have been discussed. In particular, when either the UAV trajectory or commanded rates across single-hop links is fixed, then the resulting constraint set and cost function are convex. For both single- and multiple-user scenarios we have shown that significant energy savings, upwards of 70% in some cases, are available through joint control of propulsion and transmission.

Immediate extensions of this work include higher fidelity models. Considering a goal of on-line real-time control of multi-agent networks, the following key developments must be addressed: (i) Closed-loop analysis of the control strategy in a decreasing or variable horizon framework, encompassing error propagation analysis; (ii) A robust, distributed framework for the problem, to include the use of adaptive models.

All energy expenditure on an autonomous agent may be categorized as being due to propulsion, communication or computation. Considering the tangible trade-off between computation and communication energy [3], [32], a more distant

consideration is to include computation energy, such as due to data compression or aggregation [41], into the problem.

REFERENCES

- [1] J. Ko, A. Mahajan, and R. Sengupta, "A network-centric UAV organization for search and pursuit operations," in *Proc. IEEE Aerospace Conf.*, vol. 6, pp. 6–6, 2002.
- [2] S. Wang, A. Gasparri, and B. Krishnamachari, "Robotic message ferrying for wireless networks using coarse-grained backpressure control," in *IEEE Globecom Workshops*, pp. 1386–1390, 2013.
- [3] M. Thammawichai, S. P. Baliyarasimhuni, E. C. Kerrigan, and J. B. Sousa, "Optimizing communication and computation for multi-UAV information gathering applications," *IEEE Transactions on Aerospace and Electronic Systems*, vol. 54, no. 2, pp. 601–615, 2018.
- [4] P. Zhan, K. Yu, and A. L. Swindlehurst, "Wireless relay communications with unmanned aerial vehicles: Performance and optimization," *IEEE Transactions on Aerospace and Electronic Systems*, vol. 47, no. 3, pp. 2068–2085, 2011.
- [5] I. Bekmezci, O. K. Sahingoz, and Ş. Temel, "Flying ad-hoc networks (FANETs): A survey," *Ad Hoc Networks*, vol. 11, no. 3, pp. 1254–1270, 2013.
- [6] S. Zhang, Y. Zeng, and R. Zhang, "Cellular-enabled uav communication: Trajectory optimization under connectivity constraint," *arXiv preprint arXiv:1710.11619*, 2017.
- [7] M. Mozaffari, W. Saad, M. Bennis, and M. Debbah, "Wireless communication using unmanned aerial vehicles (UAVs): Optimal transport theory for hover time optimization," *IEEE Transactions on Wireless Communications*, vol. 16, no. 12, pp. 8052–8066, 2017.
- [8] M. Mozaffari, W. Saad, M. Bennis, and M. Debbah, "Unmanned aerial vehicle with underlaid device-to-device communications: Performance and tradeoffs," *IEEE Transactions on Wireless Communications*, vol. 15, no. 6, pp. 3949–3963, 2016.
- [9] Y. Zeng, R. Zhang, and T. J. Lim, "Throughput maximization for mobile relaying systems," *IEEE Trans. Communications*, vol. 64, no. 12, pp. 4983–4996, 2016.
- [10] Y. Zeng and R. Zhang, "Energy-efficient UAV communication with trajectory optimization," *IEEE Trans. Wireless Communications*, vol. 16, pp. 3747 – 3760, June 2017.
- [11] Y. Yan and Y. Mostofi, "To go or not to go: On energy-aware and communication-aware robotic operation," *IEEE Transactions on Control of Network Systems*, vol. 1, no. 3, pp. 218–231, 2014.
- [12] Q. Wu, J. Xu, and R. Zhang, "Capacity characterization of uav-enabled two-user broadcast channel," *IEEE Journal on Selected Areas in Communications*, vol. 36, no. 9, pp. 1955–1971, 2018.
- [13] D. Yang, Q. Wu, Y. Zeng, and R. Zhang, "Energy tradeoff in ground-to-uav communication via trajectory design," *IEEE Transactions on Vehicular Technology*, vol. 67, no. 7, pp. 6721–6726, 2018.
- [14] Q. Wu, Y. Zeng, and R. Zhang, "Joint trajectory and communication design for multi-uav enabled wireless networks," *IEEE Transactions on Wireless Communications*, vol. 17, no. 3, pp. 2109–2121, 2018.
- [15] J. Lyu, Y. Zeng, and R. Zhang, "Cyclical multiple access in UAV-aided communications: A throughput-delay tradeoff," *IEEE Wireless Communications Letters*, vol. 5, no. 6, pp. 600–603, 2016.
- [16] D. Tse and P. Viswanath, *Fundamentals of wireless communication*. Cambridge university press, 2005.
- [17] Y. Yan and Y. Mostofi, "Robotic router formation in realistic communication environments," *IEEE Transactions on Robotics*, vol. 28, no. 4, pp. 810–827, 2012.
- [18] U. Ali, Y. Yan, Y. Mostofi, and Y. Wardi, "An optimal control approach for communication and motion co-optimization in realistic fading environments," in *American Control Conference (ACC), 2015*, pp. 2930–2935, IEEE, 2015.
- [19] U. Ali, H. Cai, Y. Mostofi, and Y. Wardi, "Motion and communication co-optimization with path planning and online channel estimation," in *Proc. 2016 American Control Conference*, July 2016.
- [20] O. J. Faqir, E. C. Kerrigan, and D. Gündüz, "Joint optimization of transmission and propulsion in aerial communication networks," in *Decision and Control (CDC), 2017 IEEE 56th Annual Conference on*, pp. 3955–3960, IEEE, 2017.
- [21] O. J. Faqir, N. Yuanbo, E. C. Kerrigan, and D. Gündüz, "Energy-efficient communication in mobile aerial relay-assisted networks using predictive control," in *Nonlinear Model Predictive Control (NMPC), 2018 IFAC 6th Conference on*, IFAC, 2018.
- [22] P. Sujit, S. Saripalli, and J. B. Sousa, "Unmanned aerial vehicle path following: A survey and analysis of algorithms for fixed-wing unmanned aerial vehicles," *IEEE Control Systems*, vol. 34, no. 1, pp. 42–59, 2014.
- [23] Y. Kang and J. K. Hedrick, "Linear tracking for a fixed-wing UAV using nonlinear model predictive control," *IEEE Transactions on Control Systems Technology*, vol. 17, no. 5, pp. 1202–1210, 2009.
- [24] D. Gunduz and E. Erkip, "Opportunistic cooperation by dynamic resource allocation," *IEEE Transactions on Wireless Communications*, vol. 6, no. 4, 2007.
- [25] D. N. C. Tse and S. V. Hanly, "Multiaccess fading channels. I: Polymatroid structure, optimal resource allocation and throughput capacities," *IEEE Transactions on Information Theory*, vol. 44, no. 7, pp. 2796–2815, 1998.
- [26] A. T. Schwarm and M. Nikolaou, "Chance-constrained model predictive control," *AICHe Journal*, vol. 45, no. 8, pp. 1743–1752, 1999.
- [27] Y. Mei, Y.-H. Lu, Y. C. Hu, and C. G. Lee, "Energy-efficient motion planning for mobile robots," in *Proc. IEEE Int'l Conf. on Robotics and Automation*, pp. 4344–4349, 2004.
- [28] P. Tokekar, N. Karnad, and V. Isler, "Energy-optimal trajectory planning for car-like robots," *Autonomous Robots*, vol. 37, no. 3, pp. 279–300, 2014.
- [29] J. Anderson, *Introduction to Flight*. McGraw-Hill, 2015.
- [30] M. Mozaffari, W. Saad, M. Bennis, and M. Debbah, "Mobile unmanned aerial vehicles (UAVs) for energy-efficient internet of things communications," *IEEE Trans. Wireless Communications*, vol. 16, pp. 7574–7589, November 2017.
- [31] Y. Nie, O. J. Faqir, and E. C. Kerrigan, "ICLOCS2: Solve your optimal control problems with less pain," in *Proc. 6th IFAC Conference on Nonlinear Model Predictive Control*, 2018.
- [32] S. Nazemi, K. K. Leung, and A. Swami, "QoI-aware tradeoff between communication and computation in wireless ad-hoc networks," in *Personal, Indoor, and Mobile Radio Communications (PIMRC), 2016 IEEE 27th Annual International Symposium on*, pp. 1–6, IEEE, 2016.
- [33] S. Boyd and L. Vandenberghe, *Convex optimization*. Cambridge University Press, 2004.
- [34] G. Debreu and T. C. Koopmans, "Additively decomposed quasiconvex functions," *Mathematical Programming*, vol. 24, no. 1, pp. 1–38, 1982.
- [35] S. Wolf, "An introduction to duality in convex optimization," *Network*, vol. 153, 2011.
- [36] M. Kelly, "An introduction to trajectory optimization: how to do your own direct collocation," *SIAM Review*, vol. 59, no. 4, pp. 849–904, 2017.
- [37] A. Wächter and L. Biegler, "On the implementation of an interior-point filter line-search algorithm for large-scale nonlinear programming," *Mathematical Programming*, vol. 106, pp. 25–57, Mar 2006.
- [38] Y. Nie and E. C. Kerrigan, "How should rate constraints be implemented in nonlinear optimal control solvers?," in *Proc. 6th IFAC Conference on Nonlinear Model Predictive Control*, 2018.
- [39] D. Gunduz, K. Stamatiou, N. Michelusi, and M. Zorzi, "Designing intelligent energy harvesting communication systems," *IEEE Communications Magazine*, vol. 52, no. 1, pp. 210–216, 2014.
- [40] Y. Zhou, J. Li, L. Lamont, and C.-A. Rabbath, "Modeling of packet dropout for UAV wireless communications," in *Computing, Networking and Communications (ICNC), 2012 International Conference on*, pp. 677–682, IEEE, 2012.
- [41] O. Orhan, D. Gündüz, and E. Erkip, "Source-channel coding under energy, delay, and buffer constraints," *IEEE Transactions on Wireless Communications*, vol. 14, no. 7, pp. 3836–3849, 2015.